# CFD-FSI analysis of two-dimensional Thermo-Elasto-Hydrodynamic Lubrication contacts

P. Havaej [a], J. Degroote [b, c], D. Fauconnier [a, c*]

[a] *Soete Laboratory, Department of Electromechanical, Systems & Metal Engineering, Faculty of Engineering and Architecture, Ghent University, Technologiepark 903, 9052 Zwijnaarde, Belgium*

[b] *STFES, Department of Electromechanical, Systems & Metal Engineering, Faculty of Engineering and Architecture, Ghent University, Sint-Pietersnieuwstraat 41, 9000 Ghent, Belgium*

[c] *Flanders Make @ UGent – Core Lab EEDT-MP*

## Abstract

In this study, the numerical modelling of the Thermo-Elasto-Hydrodynamic Lubrication (TEHL) contact is investigated. Flow model, structure, and lubricant rheology models have been developed in the OpenFOAM (extend version) package. Regarding complex and cavitating flow in TEHL contact, a Homogeneous Equilibrium Model (HEM) is used, including the thermal effect and variation in lubricant properties due to pressure, temperature, and shear rate. Besides the linear elastic equation, the heat conduction equation is solved to describe the solid deformation and temperature distribution in the solid domain. Furthermore, a partitioned Fluid-structure interaction (FSI) methodology is employed to make a two-coupling between fluid and solid regions. Also, along with FSI modelling, a Conjugate Heat Transfer (CHT) simulation is essential to precisely investigate the thermal behaviour of TEHL contacts. The developed TEHL model shows properly the involved physics in comparison with acceptable data for rolling-sliding 2D line contacts from the literature and provides trustworthy results in different operating conditions. Three different slide to roll ratios are considered. The variation in lubricant film, pressure, temperature, and viscosity are discussed in detail. Also, analysis of von Mises stress in solid materials shows that the TEHL model predicts the location of maximum stress like traditional Hertzian contact theory.

**Keywords:** Thermo-Elastohydrodynamic Lubrication (TEHL), Computational Fluid Dynamics (CFD), Fluid-Structure Interaction (FSI), Cavitation, OpenFOAM

[*] Corresponding author. Address: Department of Electromechanical, Systems and Metal Engineering, Faculty of Engineering and Architecture, Ghent University, Ghent, Belgium. Emails: dieter.fauconnier@ugent.be

## 1. Introduction

Lubrication is vital to improve performance, durability, and reduce the cost of machine elements. The primary role of lubrication is to separate (fully or partially) the opposing surfaces of interacting machine elements. This study focuses on the Elasto-Hydrodynamic Lubrication (EHL) regime. EHL is characterized by very thin lubricant films ($50nm-1\mu m$) and locally extreme hydrodynamic pressures (up to $1-4\ GPa$). Compressive heating and shear heating become important at high contact loads and sliding speeds in gears and bearing contacts. In this case, thermal effects have a major influence on viscosity and lubricant properties at the contact. Hence, this lubricant regime is well-known as Thermo-Elastohydrodynamic Lubrication (TEHL), which exists widely in helical and worm gears, roller and needle bearings, cam/follower systems, hydraulic pumps, and metal-rolling tools.

The classical Reynolds-Boussinesq approach is mostly used to model EHL contacts [1,2]. Although the Reynolds equation has shown an appropriate accuracy and computational time, it is mainly limited to isothermal EHL [3,4]. Different modified Reynolds equations were presented to include the thermal effects, which used averaged lubricant properties over the film-thickness [5]. However, Computational Fluid Dynamics (CFD) has shown that it can be a powerful tool for TEHL problems to investigate lubricated contacts in detail and accurately in recent years. Conservation equations for mass, momentum, and energy are solved along with proper constitutive equations for thermomechanical properties of the lubricant. Moreover, a linear elastic solver or an elasto-static boundary element method is used to describe the stresses and deformation in the solid bodies.

In 2000, Schäfer et al. [3] were pioneers in the simulation of an EHL contact by solving the Stokes flow equations instead of the Reynolds equation. However, they neglected the non-Newtonian effects, liquid compressibility, and thermal effects. Bruyere et al. [6] proposed a single-phase flow CFD model as well as a Finite Element solver for the structural part for steady-state simulation of TEHL contacts. Their study provided an understanding of thermal behaviour and the flow pattern in contact. They reported that in pure sliding, the solid thermal conductivity could influence the local shear forces. Hartinger et al. [7] performed a preliminary study on using the CFD technique in a 2D line TEHL contact, including thermal, cavitation, liquid compressibility, and non-Newtonian effects. They have reported a very good agreement between the CFD model and the Reynolds solution in different operating conditions. Also, a thermal validation of this model for 3D point TEHL contact was presented later [8]. Hajishafiee et al. [9] developed Hartinger's model and considered a linear elastic structural model for the solid body in order to make a strong FSI coupling between fluid and solid domains. They showed that this approach is applicable for the simulation of practical conditions for rolling element bearings.

The current study aims to develop a 2D CFD-FSI solver for TEHL of line contacts in OpenFOAM, including liquid compressibility, non-Newton behaviour, conjugate heat transfer and cavitation, and provide validation for the developed solver. An equivalent geometry of a 2D line contact can be considered using the elastic half-space theory [10], in which a solid cylinder is rolling over a flat surface. Regarding complex and cavitating flow in TEHL contact, a Homogeneous Equilibrium Model (HEM) model is explained in detail. This model can incorporate the thermal effect as well as variation in lubricant properties due to pressure, temperature and shear rate. Moreover, a linear elastic solver in combination with a temperature equation are employed to describe deformation and heat conduction through the solids materials. In analogy with the work of Hartinger et al. [7] and Hajishafiee et al. [9], a 2D CFD-FSI solver for TEHL has been developed at UGent, but with a focus on improved modelling to account for the variation of thermal

properties, accurate rheology models, and precisely thermal models. A partitioned Fluid-structure interaction (FSI) methodology is employed to make a two-way coupling between fluid and solid regions. The conservation equations for both fluid and solid representative for the TEHL-physics involved are discretized by the Finite Volume (FV) approach, using a cell-centred collocated arrangement of the primitive variable. The numerical implementation was performed by developing a new solver and library for lubricant properties in the OpenFOAM (Open-source Field Operation And Manipulation) framework. Different operating conditions are considered; the variation in lubricant film, temperature, and viscosity are studied.

## 2. Flow model description

A schematic view of the 2D line contact geometry for a cylinder over a flat plate is presented in Figure 1. The lubricant is pressurized in a converging zone generating a high-pressure zone and a clearance between the surfaces. In the diverging region, the pressure drops suddenly, and cavitation can be observed there.

(a)

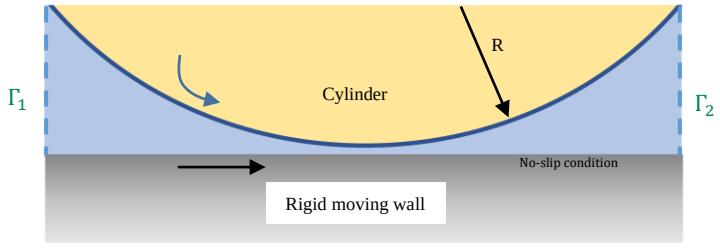


Figure 1 A schematic view of the 2D geometry.

### 2.1. Governing equations

For the description of the lubricant cavitation, the model of Karrholm and Weller [11] has been used, combining a Homogeneous Equilibrium Model (HEM) with a barotropic Equation of State (EoS). All governing equations for fluid motion are listed in Table 1, including conservation of mass, momentum, and energy. It should be pointed out that the mixture dynamic viscosity, heat capacity, compressibility are assumed to be a linear weighted average of both phase fractions. Although the phase change is primarily governed by a decrease in pressure, hence the name barotropic EoS, temperature effects are included in phase density; hence, the EoS depends on both pressure and temperature. In literature, different models can also be found for the mixture density [12,13]. Regarding the energy equation, equation (4) has been used for the mixture temperature based on the studies of Hartinger et al. [7,8,14] and Hajishafiee [9,15].

Table 1 Fluid equations.

| Description | Equation | |
|---|---|---|
| Mass conservation | $\frac{\partial \rho}{\partial t} + \nabla \cdot (\rho u) = 0$ | (1) |
| Momentum equation | $\frac{\partial (\rho u)}{\partial t} + \nabla \cdot (\rho u u) - \nabla \cdot \tau = -\nabla \cdot p$ | (2) |
| Viscous stress tensor | $\tau = \mu(\nabla u + (\nabla u)^T)\mu\frac{2}{3} I \nabla \cdot u$ | (3) |

| | | |
|---|---|---|
| Energy equation | $\rho C_p \frac{DT}{Dt} + \frac{D\alpha_v}{Dt}(\rho_v h_v - \rho_l h_l) = \nabla \cdot (k_{eff} \nabla T) - \tau : \nabla u + \alpha_v \frac{DP}{Dt} + \alpha_l \beta T \frac{DP}{Dt}$ | (4) |
| Mixture density | $\rho = \psi (p - p_{sat}) + \alpha_l \rho_{l,0} + (\alpha_v \psi_v + \alpha_l \psi_{l,M}) p_{sat}$ | (5) |
| Vapor volume fraction | $\alpha_v = \frac{\rho - \rho_{l,sat}}{\rho_{v,sat} - \rho_{l,sat}}$ | (6) |
| Mixture compressibility | $\psi = \alpha_v \psi_v + \alpha_l \psi_{l,M}$ | (7) |
| Vapor density | $\rho_v = \psi_v p$ | (8) |
| Liquid density | $\rho_l = \rho_{l,0} + \psi_{l,M} p$ | (9) |
| Liquid average compressibility | $\psi_{l,M}(p,T) = \frac{1}{p - p_{sat}} \int_{p_{sat}}^{p} \psi_l(p',T) dp' = \frac{1}{p - p_{sat}} \int_{p_{sat}}^{p} \left(\frac{\partial \rho_l}{\partial p'}\right)_s dp'$ | (10) |

In this study, the Tait-equation is employed as an equation of state for the liquid phase of the lubricant. This model has shown a good agreement with experimental data, especially at high pressure concerning TEHL contacts [16]. The dependency of viscosity to pressure and temperature is described by the Doolittle model [17]. Furthermore, the non-Newtonian behaviour of lubricant is explained by the modified Carreau model proposed by Bair [16]. In this model, limiting shear stress, as presented in equation (18), should be used to avoid unphysical viscosity values. Constitutive models are presented in Table 2.

Moreover, at a pressure in orders of magnitude of GPa, the thermal properties are not constant; hence, equations of (19)-(22) include pressure and temperature influences on heat conductivity and heat capacity of lubricant [18,19].

Table 2 Constitutive equations.

| Description | Equation | |
|---|---|---|
| Tait equation of state | $\rho_{Tait} = \rho_0 \left( \frac{1}{V_0/V_R} \times \frac{1}{V/V_0} \right)$ | (11) |
| Ratio of the fluid volume at pressure P relative to the volume at ambient pressure | $\frac{V}{V_0} = 1 - \frac{1}{1 + \acute{K}_0} ln \left[ 1 + \frac{P}{K_0} (1 + \acute{K}_0) \right]$ | (12) |
| Bulk modulus at ambient pressure | $K_0 = K_{00} exp^{-\beta K T}$ | (13) |
| The volume of the liquid at ambient pressure relative to the volume at the reference state | $\frac{V_0}{V_R} = 1 + a_V (T - T_R)$ | (14) |

| | | |
|---|---|---|
| Doolittle viscosity model for pressure and temperature dependency | $\mu_{Doolittle} = \mu_R \exp\left( B\ R_0 \left( \frac{\frac{V_\infty}{V_{\infty,R}}}{\frac{V}{V_R} - R_0 \frac{V_\infty}{V_{\infty,R}}} \right) - \frac{1}{1 - R_0} \right)$ | (15) |
| Relative occupied volume | $\frac{V_\infty}{V_{\infty,R}} = 1 + \varepsilon(T - T_R)$ | (16) |
| Shifted Carreau shear thinning model | $\eta_{Shifted-Carreau}(T, P, \dot{\gamma}) = \mu \left[ 1 + \left( \dot{\gamma} \lambda_R \frac{\mu}{\mu_R} \frac{T_R}{T} \frac{V}{V_R} \right)^2 \right]^{(n-1)/2}$ | (17) |
| Limiting shear stress model | $\tau_L = \Lambda\, p$ | (18) |
| Thermal conductivity | $\kappa = \frac{V}{V_R} \left( 1 + A \left( \frac{T}{T_R} \right) \left( \frac{V}{V_R} \right)^3 \right)$ | (19) |
| | $k = C + B\kappa^{-s}$ | (20) |
| Heat capacity | $\chi = \left( \frac{T}{T_R} \right) \left( \frac{V}{V_R} \right)^{-4}$ | (21) |
| | $\rho C_P = C_0 + m\chi$ | (22) |

In order to calculate stresses and deformation in a solid body, the well-known Navier–Cauchy equation for moderate stresses and strains are used, which are provided in Table 3. Note that heat conduction in the moving solid materials is presented in equation (26), which is solved along with the fluid energy conservation equation to obtain the solid temperature field.

Table 3 Solid equations.

| Description | Equation | |
|---|---|---|
| Navier–Cauchy equation | $\rho_s \frac{\partial^2(v)}{\partial t^2} - \nabla \cdot \left[ \mu_s \nabla v + \mu_s (\nabla v)^T + \lambda_s I \left( tr(\nabla v) \right) \right] = \rho_s f_b$ | (23) |
| Lame's coefficients | $\mu_s = \frac{E}{2(1 + \vartheta)}$ | (24) |
| | $\lambda_s = \frac{\vartheta E}{(1 + \vartheta)(1 - 2\vartheta)}$ | (25) |
| Heat conduction in the moving solid | $\rho_s C_s \frac{\partial T}{\partial t} + \dot{v_s}.\nabla T = \nabla \cdot (k_s\, \nabla T)$ | (26) |

Based on the second Newton's law, the external load ($W_{ext}$) exerted on the contact pair should be balanced by the hydrodynamic load resultant from the generated pressure in the lubricant film, W, which is calculated by integrating the pressure over the roller surface. To ensure that the load balance is satisfied, the proper rigid displacement of the rigid plate is calculated iteratively using equation (27).

$$\Delta h_d = (v_{max} - v_{min}) \frac{W_{ext} - W}{W_{ext}} \frac{\Delta t}{t_d}\, r_d \tag{27}$$

Where $\Delta h_d$ is the increment in rigid displacement calculated in each iteration, and $t_d = {}^{R}/_{a_s}$ is a characteristic deformation time, $a_s$ is the sonic velocity in the solid material, $r_d$ is an under-relaxation factor, $v_{max}$ and $v_{min}$ are the maximum and minimum deformation in the solid body, respectively [9,15].

Regarding the mesh motion, a finite volume solver is employed in which the instance velocities of points is calculated based on the Laplacian operator as below:

$$\nabla.(\gamma\nabla\vec{u}) = 0 \tag{28}$$

Where u is the velocity of points, and the new position of points can be calculated as follows:

$$\vec{x}_{new} = \vec{x}_{old} + \vec{u}\Delta t \tag{29}$$

Hence, the mesh is modified by displacement increment. Moreover, an exponential diffusivity model is used for the Laplacian solver.

$$\gamma = \exp^{-\alpha/l} \tag{30}$$

where l is the distance to the prescribed boundary.

### 2.2. Boundary conditions

The static pressure is fixed at $\Gamma_1$ (inlet), and $\Gamma_2$ (outlet) boundaries of the domain (please see Figure 1), whereas the "pressureInletOutlet" boundary condition is considered for the velocity field. Also, No-slip boundary conditions are applied for the fluid velocity at the solid walls, and Neumann boundary conditions are imposed for the pressure there. For the temperature equation, the "inletOutlet" condition is applied at the inlet, while the Neumann condition is used at the outlet since an outflow condition is observed in studied cases. Also, a mixed boundary condition is required on both sides of the fluid-solid interface to ensure that the same heat flux passes through fluid and solid domains and the temperature of lubricant and solid at the interface are the same.

For the rigid wall sliding over the contact, the Carslaw-Jaeger temperature boundary condition is used, which has been suggested for TEHL contacts [20,21]. It has been derived for a moving point heat source for a semi-infinite body. In a 2D line contact, the temperature is:

$$T_{Cars} = \sqrt{\frac{1}{\pi\rho_s C_s K_s U_s}} \int_{-\infty}^{x} q_f(\hat{x}) \frac{d\hat{x}}{\sqrt{x-\hat{x}}} \tag{31}$$

This boundary can be used for Peclet number greater than 5, $Pe = \frac{LU_s}{\alpha_T} > 5$, which is fully satisfied in this study. Besides challenging in implementation, this is a time-consuming part of the solver; however, it still requires less computational effort than solving heat conduction in the second body.

For structural solver, "solidTraction" boundary condition is used, which enables to use of lubricant pressure and torsion forces at interface.

### 2.3. FSI procedure

A partitioned approach has been applied to couple the fluid and solid solvers, in which the interface displacement is determined using an Aitken or filtered IQN-ILS algorithm [22,23]. Between 4 to 8 iterations are required to reach convergence up to $10^{-8}$ in each time step. A schematic of the coupling approach is illustrated in Figure 2. In this two-way FSI coupling, the displacement is transferred from the solid to the fluid domain, whereas the pressure and shear forces are transferred

from fluid to the solid domain. Indeed, the temperature and heat flux are also transferred between regions as the heat flux consistency with no temperature jump at the interface is satisfied.

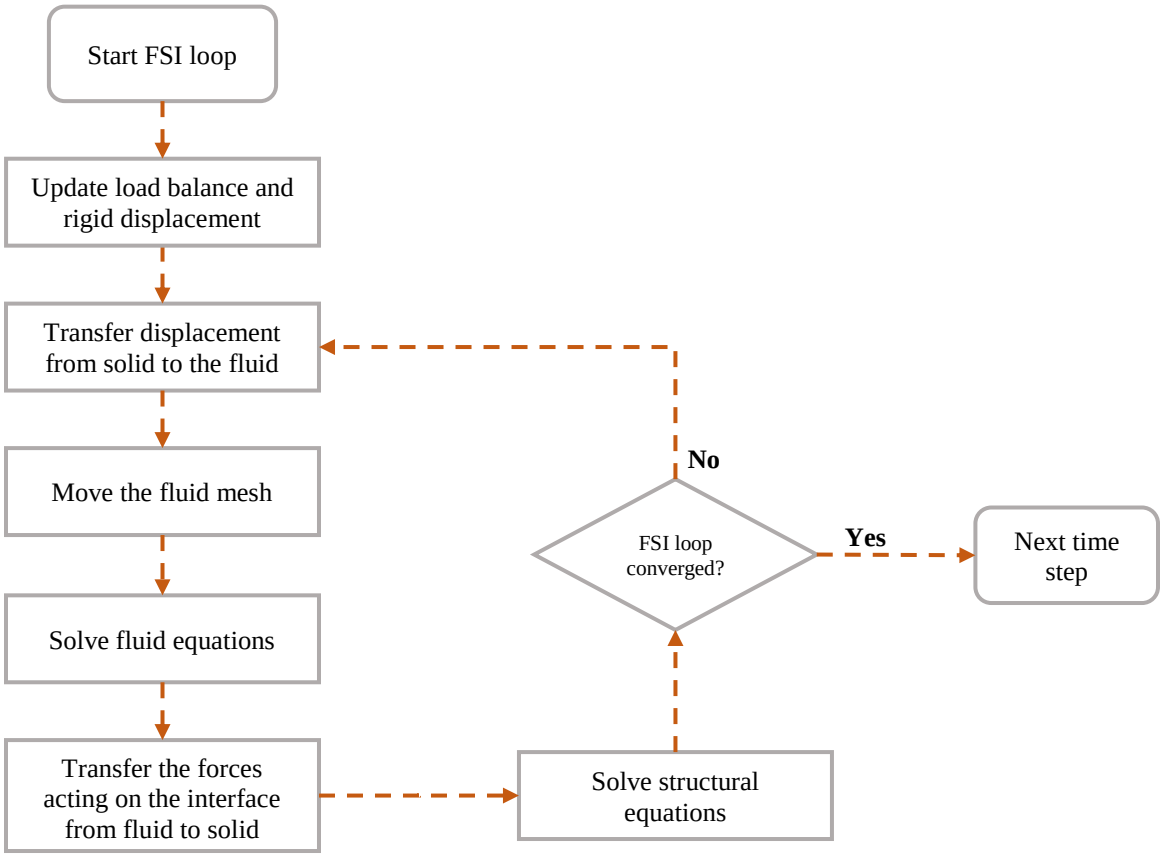


Figure 2 Flow chart of the FSI coupling algorithm.

## 3. Numerical procedure

The HEM model and thermomechanical properties libraries have been implemented in OpenFOAM extended version 4.1. Also, the fluid and structural solvers were developed by the authors to take all essential parts of TEHL modelling into account. For the fluid-solid interaction problems, the solids4Foam toolbox developed by Cardiff et al. [24–26] has been employed to make a coupling between the fluid and solid domain.

The fluid conservations equation and Navier–Cauchy equation were discretized by the Finite Volume Method (FVM) for both solid and fluid domains. Using a steady-state simulation leads to convergence issues in fluid and consequently the interface algorithm; hence, a pseudo transient simulation has been performed to prevent convergence issues and keep the computational time acceptable. In this study, the SLTS (Stabilized local time-step) time integration scheme has been employed. A time step value in the order of magnitude of $10^{-9}$ – $10^{-10}$ s was also essential for stability reasons, and the PIMPLE algorithm with 5-10 outer iterations was employed for the mixture pressure-velocity coupling. The runtime of the code to achieve a steady-state condition is between 12-16 days in serial mode, and it is between 5-7 days for parallel mode with 6 processors. Indeed, the runtime depends on the operating condition, type of lubricant, mechanical factors, etc. Worth noting that a full transient simulation of TEHL contacts required at least two times the above-mentioned computational times. Moreover, the solid solver uses almost half of the

computational time, which is mainly because of using finite volume technique and segregated solution algorithm for structural simulation, which suffers from a slow convergence rate [26].

The load balancing explained in equation (27) was implemented using the swak4Foam package and "groovyBC" boundary condition, enabling better control of rigid displacement and access to boundary values.

A part of the computational grid is revealed in Figure 3. The mesh was generated by the blockMeshDict utility. Several blocks were defined to control mesh quality, skewness better and refine mesh at a high gradient area at the contact. The solid mesh was also generated accordingly to minimize the interpolation error at the non-conformal fluid/solid interface. It should be noted that it has been found that 10000 cells in fluid and 20000 cells in solid are required.

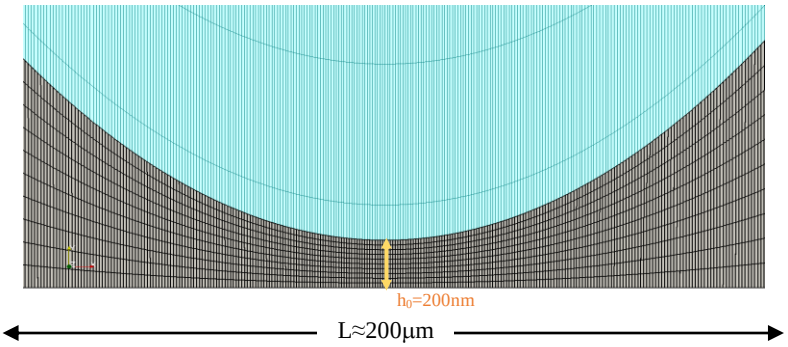


Figure 3 Computational grid at the contact, grey colour is the fluid domain, and blue colour shows solid domain.

## 4. Results

The selected lubricant is Squalane because of the availability of properties data in the literature [27,28] and fine-tuned parameters for EoS, viscosity, and thermal properties models [18,29]. All lubricant parameters are listed in Table 4-4 and solid material properties in Table 7.

Table 4 EoS parameters.

| Parameter | Value | Dimension | Parameter | Value | Dimension |
|---|---|---|---|---|---|
| **Liquid density at saturation pressure** | $\rho_{l,sat} = 794.6$ | $kg/m^3$ | **Thermal expansion defined in volume ratio** | $a_V = 8.36 \times 10^{-4}$ | $K^{-1}$ |
| **Vapour density at saturation pressure** | $\rho_{v,sat} = 0.0288$ | $kg/m^3$ | **$K_0$ at zero absolute temperature** | $K_{00} = 8.658$ | $GPa$ |
| **Saturation pressure** | $p_{sat} = 5000$ | $Pa$ | **Temperature coefficient of $K_0$** | $\beta_k = 6.332 \times 10^{-3}$ | $K^{-1}$ |
| **Rate change of isothermal bulk modulus at zero pressure** | $\acute{K}_0 = 11.74$ | - | **Inlet temperature** | $T_0 = 313.15$ | $K$ |
| | | | **Reference temperature** | $T_R = 313.15$ | $K$ |

Table 5 Viscosity and shear thinning parameters.

| Parameter | Value | Dimension | Parameter | Value | Dimension |
|---|---|---|---|---|---|
| **Dynamic viscosity vapor** | $\mu_v = 8.97 \times 10^{-6}$ | $Pa\ s$ | **Occupied volume thermal expansivity** | $\varepsilon = -7.273 \times 10^{-4}$ | $K^{-1}$ |
| **Low-shear viscosity at reference state** | $\mu_{l,R} = 0.0157$ | $Pa\ s$ | **Liquid critical shear stress or shear modulus of lubricant** | $G_{c,0} = 6.94$ | $MPa$ |
| **Doolittle parameter** | $B = 4.71$ | - | **Power law exponent** | $n = 0.463$ | - |
| **Occupied volume fraction at reference state, $T_R$, p = 0** | $R_0 = 6568$ | - | **Limiting stress pressure coefficient** | $\Lambda$=0.075 | - |

Table 6 Thermal properties parameters.

| Parameter | Value | Dimension | Parameter | Value | Dimension |
|---|---|---|---|---|---|
| **Parameter in the heat capacity function** | $m = 0.62 \times 10^6$ | $\frac{J}{m^3\ K}$ | **Parameter in the conductivity function** | $C_k = 0.074$ | $\frac{W}{m\ K}$ |
| **Parameter in the heat capacity function** | $C_0 = 0.94 \times 10^6$ | $\frac{J}{m^3\ K}$ | **Exponent in the conductivity scaling model** | $s = 4.5$ | - |
| **Coefficient in the conductivity equation** | $A = -0.115$ | - | **Coefficient in the conductivity equation** | $q = 2$ | - |

Table 7 Solid material properties.

| Parameter | Value | Dimension | Parameter | Value | Dimension |
|---|---|---|---|---|---|
| **Elastic Modulus** | $E = 200$ | $GPa$ | **Specific heat capacity** | $C_{v,s} = 450$ | $\frac{J}{kg\ K}$ |
| **Density** | $\rho_s$ =8750 | $kg/m^3$ | **Thermal conductivity** | $K_s = 47$ | $\frac{W}{m\ K}$ |

## 4.1. Validation

The developed solver for (T)EHL contacts must be evaluated in different conditions for pure sliding, pure rolling, iso-thermal, and thermal conditions. This has been done by comparing the current model results against existing acceptable CFD works in the literature. Hence, five validation configurations of two different cases are considered; the first is the thermal/iso-thermal study of Hartinger et al. [7,14] with a target load of 100kN/m. The second test case was obtained from Srirattayawong [30] and Tosic et al. [31,32] with a target load of 50kN/m. The first case was simulated using OpenFOAM, while the second case used ANSYS Fluent software. Lubricant properties and operating conditions for these cases have been set regarding corresponding references.

Figure 4 clearly indicates that the current CFD-FSI results have excellent correspondence with the CFD solution presented in the literature. The five validation cases of the two cases studied here include pure rolling, pure sliding, isothermal, non-isothermal, and target load of 50kN/m and 100kN/m. It is clear from the results that the developed TEHL model in OpenFOAM represents properly the involved physics in comparison with comparable data from the literature and provides

reliable and trustworthy results. The minor differences with Hartinger's Results are mainly because of differences in structural models and thermal boundary conditions. A linear elastic model and conjugate heat transfer equation have been solved here, while Boussinesq integral and Carslaw-Jaeger boundary conditions were used to calculate deformation and temperature at roller surface, respectively.

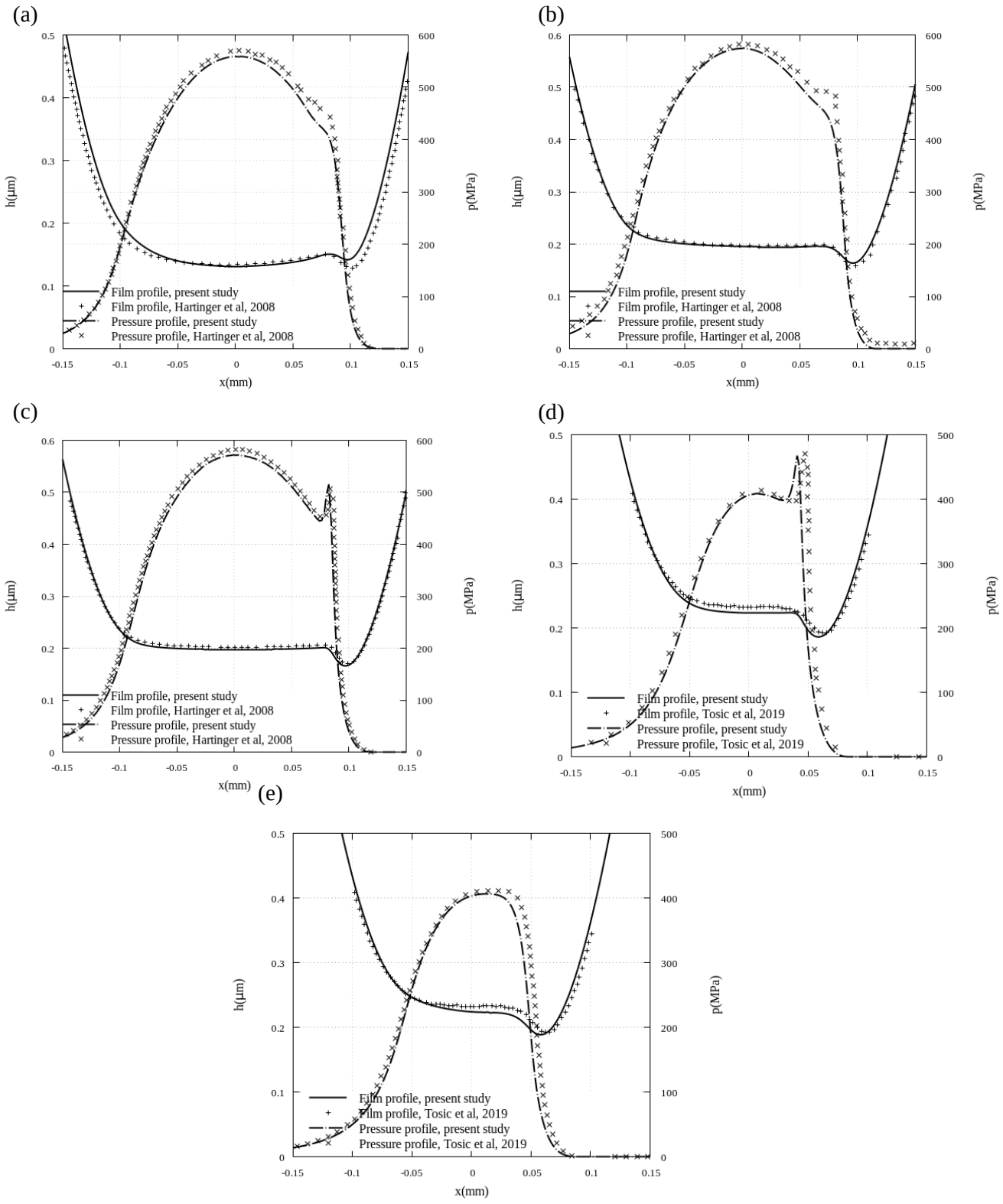


Figure 4 Validation of numerical results, for L=100kN/m, $E_r$=345.23GPa; a) SRR=2 and non-isothermal. Isothermal solution for: b) SRR=0 or pure rolling, c) SRR=2 or pure sliding. Another test case for L=50kN/m and isothermal solution of d) SRR=0, e) SRR=2.

## 4.2. Discussion

In the following, we investigate thermoelastohydrodynamic lubrication between a steel roller and a flat plate, the former subject to an external load of 100kN/m. The roller radius is 10mm, whereas the entrainment velocity is 2.5 m/s. Three different slide-roll-ratio's (SRR) are considered, i.e. pure rolling or SRR=0, rolling-sliding or SRR=1, and pure sliding or SRR=2. Figure 5 illustrates the lubricant film thickness, the pressure, the wall shear stress, and the heat flux profile at the roller surface for different SRR. To highlight the variation of these variables in the contact, the changes in viscosity should be explained first. In pure sliding conditions, due to higher shear rate, shear heating increases at the contact and consequently, the heat fluxes and temperature at interface increase in this condition. As it is indicated in Figure 5-d, heat is evacuated at a higher rate through the solid materials at SRR=2. However, in the case of pure rolling, the surfaces have the same velocity and then the shear rate is negligible. Hence, the temperature remains almost constant in the SRR=0 or pure rolling condition.

On the other hand, the maximum local shear stress at the lubricated surface is 8.6MPa, 20.3 MPa, and 16.5 MPa for SRR=0,1, and 2, respectively. When the temperature increases, the viscosity drops and then the wall shear stress decreases. Hence, although the shear rate is higher in SRR=2, the shear stress and friction forces can be lower for SRR=2 due to the decreased viscosity at higher temperatures.

The variation in viscosity can also influence the lubricant film and the pressure profile. The average lubricant film is 20% thicker in the rolling condition in comparison with a sliding condition, since the average viscosity is higher in the case of the pure rolling condition. Although the maximum pressure in different SRR is almost equal 570MPa, the pressure spike close to the outlet region is more significant in the case of the rolling condition, where the viscosity is higher at the outlet.

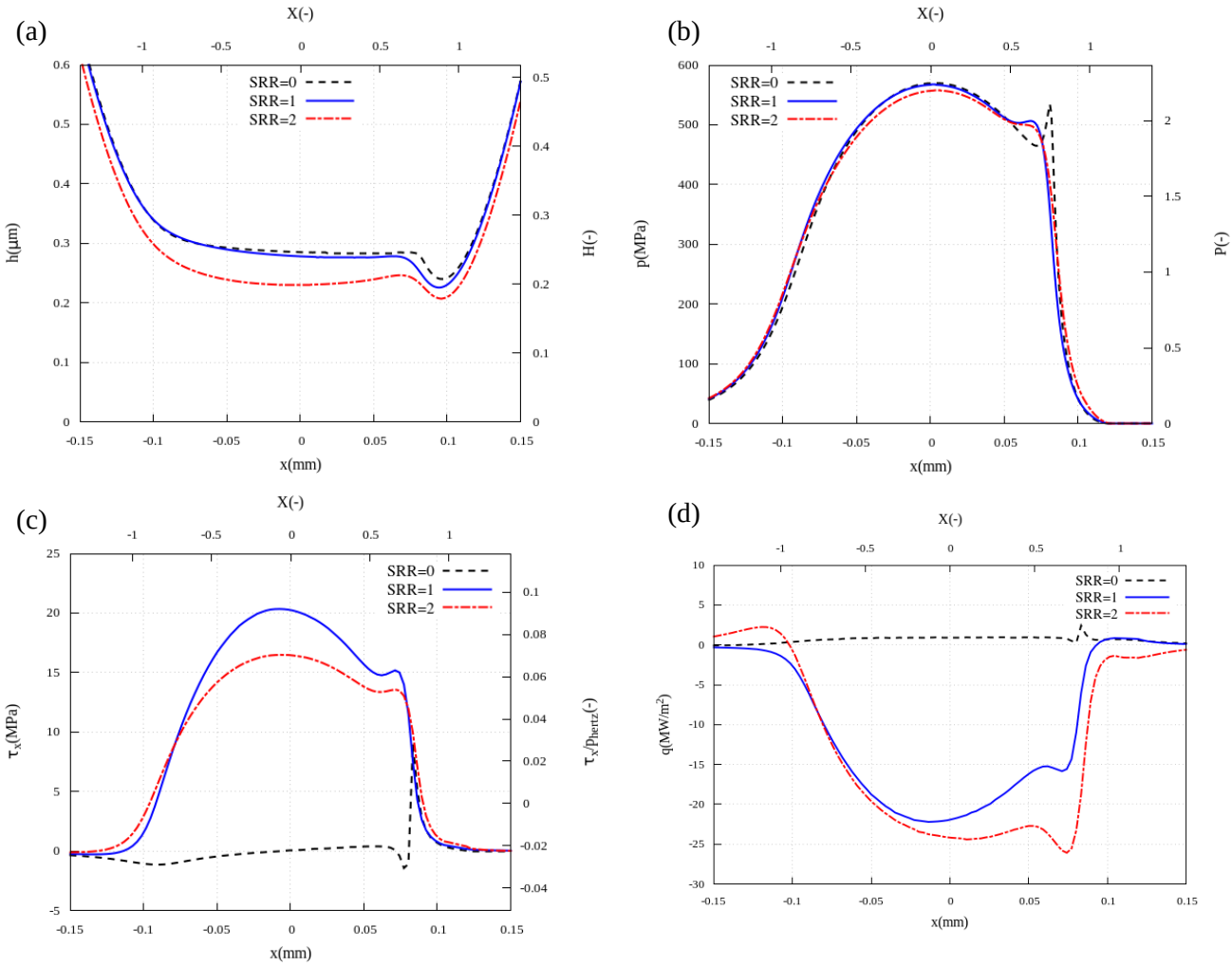


Figure 5 a) Lubricant film b) pressure c) shear stress, and d) heat flux profile at roller surface at different SRR. $L = 100\text{kN/m}, E_r = 345.23\text{GPa}$.

Figure 6 shows the temperature variation in the contact. The maximum temperature of 315K, 335.7K, and 360K are observed for SRR=0,1, and 2, respectively. Because of the very small temperature variation in SRR=0, this case has not been shown in Figure 6. Besides convection and conduction through the fluid and solid domains, the compressive work on the fluid and viscous heating play important roles in TEHL physics. In general, it has been observed that viscous heating has a dominant influence on contact temperature. Hence, viscous heating has a greater influence in pure sliding condition and a minor influence in pure rolling condition.

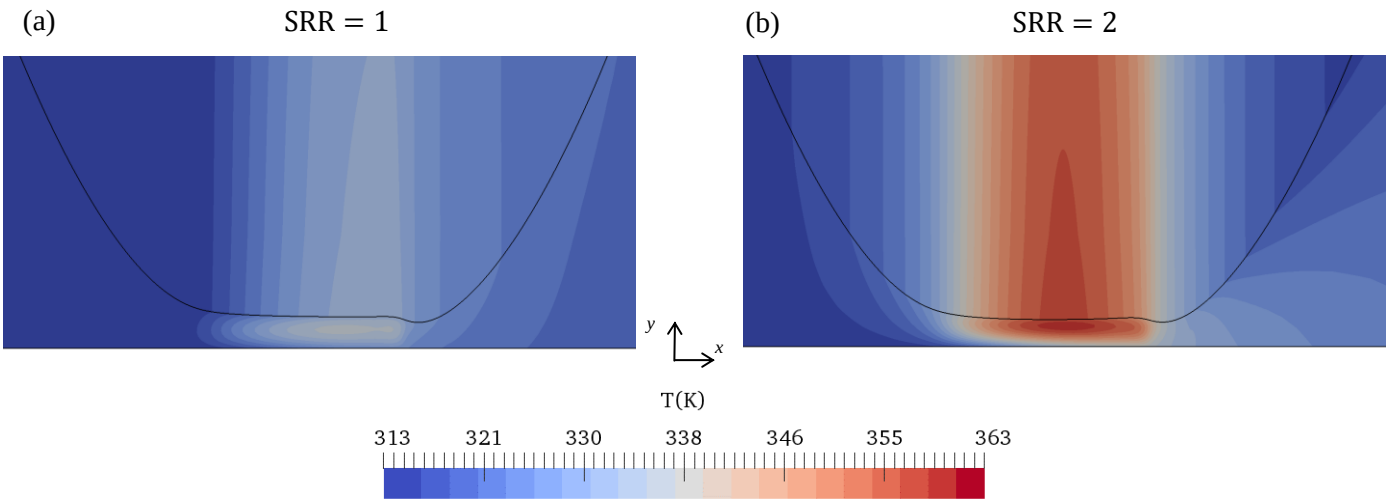


Figure 6 Temperature distribution for a) SRR=1 and b) SRR=2. $L = 100\text{kN/m}, E_r = 345.23\text{GPa}$.

The viscosity profiles are illustrated in Figure 7. It can be seen that the lubricant viscosity does not change across the film in SRR=0, confirming the validity of the one-dimensional assumption in the Reynolds equation. However, the viscosity does not remain constant across the film in SRR=1 and 2 due to temperature variation. Consequently, the one-dimensional assumption is not fully valid at these conditions. Maximum viscosity value in this operating condition is 23.5 Pa.s, 3.81 Pa.s, and 2.45Pa.s for SRR=0, 1, and 2 respectively. In addition to the temperature, the shear rate also influences significantly on the viscosity at the contact. As SRR increases, the shear rate also increases; hence, the viscosity drops to a lower value.

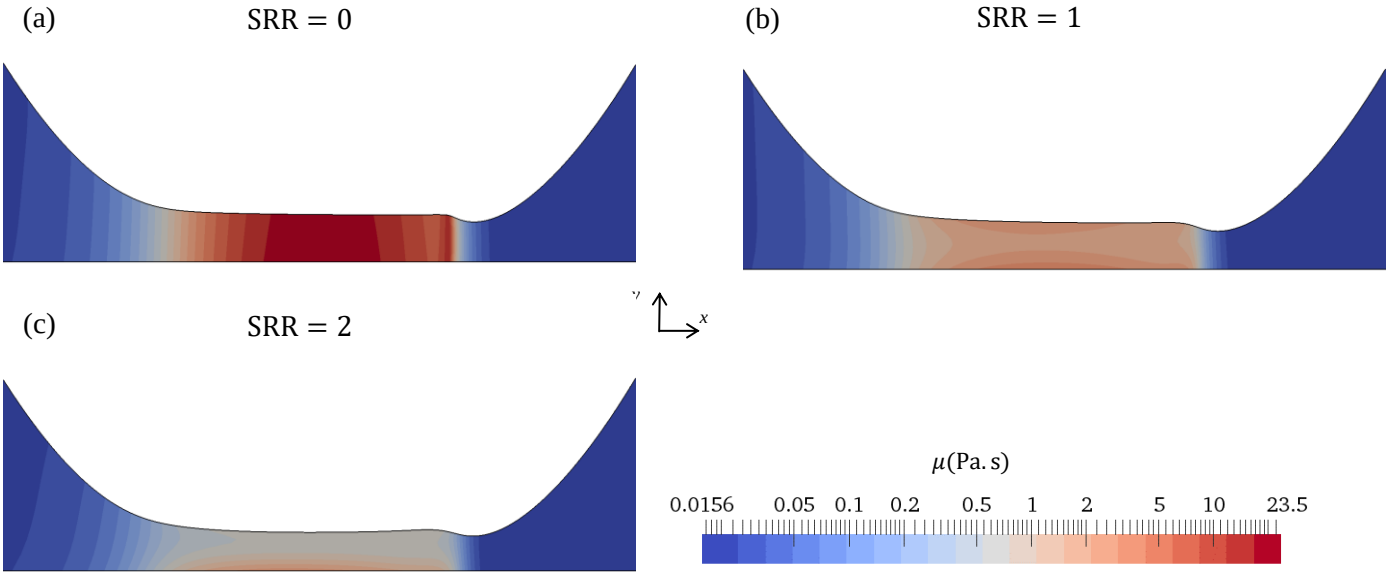


Figure 7 Viscosity distribution for a) SRR=0, b) SRR=1, and c) SRR=2. $L = 100\text{kN/m}, E_r = 345.23\text{GPa}$.

Cavitation can be observed at the outlet region of contact. The pressure increases at the centre of contact following by a sharp decrease at the outlet of contact. The cavitation can potentially occur there. Figure 8 shows the vapor volume fraction, which implies the lubricant is cavitated in the diverging region. Note that the length of cavitation is approximating 6 times half-Hertzian contact width.

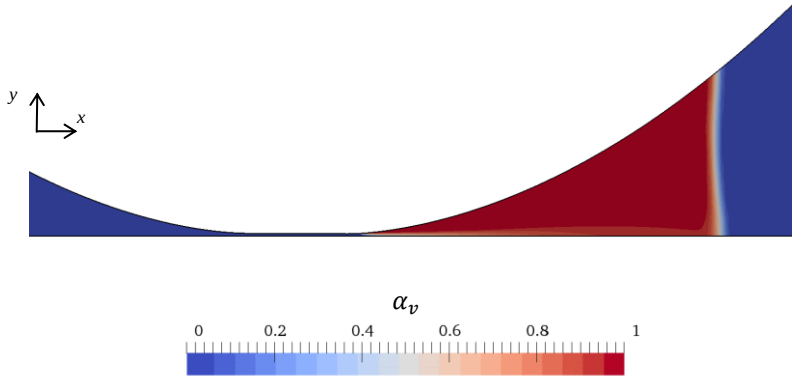


Figure 8 Vapor volume fraction.

Regarding stresses in solid materials, Figure 9 shows the von Mises stress in the roller for a smooth TEHL contact. The maximum equivalent stress of about 310MPa is observed for three studied cases. It is noteworthy that the location of maximum stress is $\frac{y}{2a} = 0.39$ away from the surface, which is in agreement with the traditional theory based on the Hertzian contact. In these cases, sub-surface failure is observed; however, if the local wall shear stress increases, the maximum von Mises stress shifts to the surface. This is however out of scope in current contribution and will be the subject of future studies.

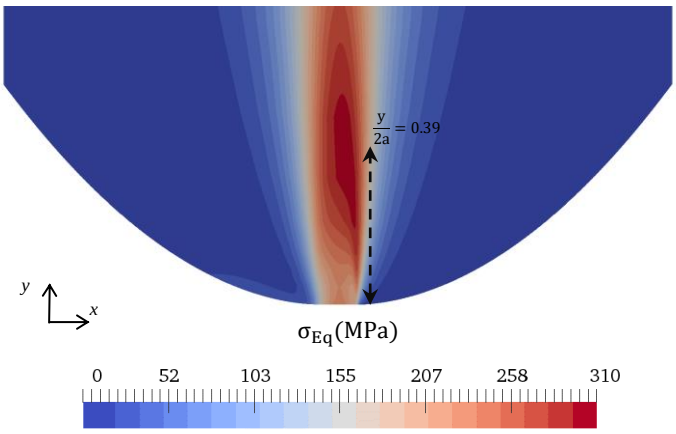


Figure 9 Von Mises stress in solid material.

A summary of numerical results is listed in Table 8. It can be observed that the maximum CoF of 0.02881 is obtained in the case of SRR=1, whereas an average thicker film with a 0.289μm thickness is calculated for SRR=0 due to previously discussed reasons.

Table 8 Summary of influence of SRR in TEHL contact.

| Case | SRR = 0 | SRR = 1 | SRR = 2 |
|---|---|---|---|
| Mean CoF on the roller (-) | 0.0004 | 0.0288 | 0.0267 |
| Max pressure (MPa) | 570.1 | 567.2 | 557.51 |
| Max shear stress in x direction (MPa) | 8.6 | 20.3 | 16.5 |
| Max temperature (K) | 315.1 | 335.7 | 360.02 |
| Minimum film thickness (μm) | 0.240 | 0.226 | 0.207 |
| Central film thickness (μm) | 0.285 | 0.278 | 0.230 |
| Average film thickness (μm) | 0.289 | 0.282 | 0.241 |
| Maximum von Mises stress (MPa) | 312.3 | 315.2 | 309.7 |
| Location of maximum von Mises stress, y/2a (-) | 0.3902 | 0.3901 | 0.3903 |

## 5. Conclusions

In this study, a CFD-FSI model for TEHL of line contacts was developed within the OpenFOAM framework, including conjugate heat transfer, Piezoviscous and non-Newtonian behaviour, cavitation, and compressibility. Rheology models have been implemented to incorporate the influence of pressure, temperature and shear rate on the lubricant properties. Also, a HEM flow solver and proper form of energy equation were adopted for this physics. The flow solver and structural model have been coupled using a two-way partitioned approach. The influence of the slide-roll-ratio (SRR) on the pressure, temperature, lubricant film, and viscosity were studied. The capability of using the CFD approach illustrated that it could include variation in temperature, viscosity and other properties across the lubricant film. Comparison of pure rolling or rolling-sliding conditions, a thicker film along with a lower coefficient of friction was calculated for pure rolling conditions, whereas a thinner film with a higher CoF and contact temperature was observed for rolling-sliding and pure sliding conditions. The advantage of the developed CFD-FSI methodology for TEHL in OpenFOAM is that it precisely provides a better and deeper physical understanding of both lubricant flow and elastic deformation of the solid surfaces. The von Mises stress was evaluated in the solid materials and found that the CFD-FSI results are in a well-agreement with traditional Hertzian contact theory. Besides precisely modelling lubricant flow and solid deformation, the developed approach can also be used to study 3D TEHL point and line contacts and the influence of surface roughness on TEHL contacts.

## References


[1] Lubrecht AA, Ten Napel WE, Bosma R. Multigrid, an alternative method of solution for two-dimensional elastohydrodynamically lubricated point contact calculations 1987.

[2] Hamrock BJ, Dowson D. Isothermal elastohydrodynamic lubrication of point contacts: Part 1—Theoretical formulation 1976.

[3] Schäfer CT, Giese P, Rowe WB, Woolley NH. Elastohydrodynamically lubricated line contact based on the Navier-Stokes equations. Tribol. Ser., vol. 38, Elsevier; 2000, p. 57–69.

[4] Scurria L, Tamarozzi T, Voronkov O, Fauconnier D. Quantitative Analysis of Reynolds and Navier–Stokes Based Modeling Approaches for Isothermal Newtonian Elastohydrodynamic Lubrication. J Tribol 2021;143. https://doi.org/10.1115/1.4050272.

[5] Dowson D. A generalized Reynolds equation for fluid-film lubrication. Int J Mech Sci 1962;4:159–70. https://doi.org/10.1016/S0020-7403(62)80038-1.

[6] Bruyere V, Fillot N, Morales-Espejel GE, Vergne P. Computational fluid dynamics and full elasticity model for sliding line thermal elastohydrodynamic contacts. Tribol Int 2012;46:3–13. https://doi.org/10.1016/j.triboint.2011.04.013.

[7] Hartinger M, Dumont M-L, Ioannides S, Gosman D, Spikes H. CFD modeling of a thermal and shear-thinning elastohydrodynamic line contact. J Tribol 2008;130:41503.

[8] Hartinger M, Reddyhoff T. CFD modeling compared to temperature and friction measurements of an EHL line contact. Tribol Int 2018;126:144–52.

[9] Hajishafiee A, Kadiric A, Ioannides S, Dini D. A coupled finite-volume CFD solver for two-dimensional elasto-hydrodynamic lubrication problems with particular application to rolling element bearings. Tribol Int 2017;109:258–73.

[10] Gohar R. Elastohydrodynamics. World Scientific; 2001.

[11] Weller H, Nordin N. Modelling injector flow including cavitation effects for diesel applications. ASME/JSME 2007 5th Jt. fluids Eng. Conf., American Society of Mechanical Engineers Digital Collection; 2007, p. 465–74.

[12] Pascarella C, Salvatore V, Ciucci A. Effects of speed of sound variation on unsteady cavitating flows by using a barotropic model. 5th Int. Symp. Cavitation CAV2003, Osaka, Jpn., 2003.

[13] Delannoy Y, Kueny JL. Two phase flow approach in unsteady cavitation modelling. Am. Soc. Mech. Eng. Fluids Eng. Div. FED, vol. 98, 1990, p. 153–8.

[14] Hartinger M. CFD modelling of elastohydrodynamic lubrication 2007.

[15] Hajishafiee A. Finite-volume CFD modelling of fluid-solid interaction in EHL contacts. Imperial College London, 2013.

[16] Bair SS. High pressure rheology for quantitative elastohydrodynamics. Elsevier; 2019.

[17] Bair S, Liu Y, Wang QJ. The pressure-viscosity coefficient for Newtonian EHL film thickness with general piezoviscous response 2006.

[18] Habchi W. A full-system finite element approach to elastohydrodynamic lubrication problems: application to ultra-low-viscosity fluids. Univ Lyon Fr 2008.

[19] Habchi W, Vergne P, Bair S, Andersson O, Eyheramendy D, Morales-Espejel GE. Influence of pressure and temperature dependence of thermal properties of a lubricant on the behaviour of circular TEHD contacts. Tribol Int 2010;43:1842–50.

[20] Kim HJ, Ehret P, Dowson D, Taylor CM. Thermal elastohydrodynamic analysis of circular contacts part 2: Non-Newtonian model. Proc Inst Mech Eng Part J J Eng Tribol 2001;215:353–62.

[21] Kim HJ, Ehret P, Dowson D, Taylor CM. Thermal elastohydrodynamic analysis of circular contacts part 1: Newtonian model. Proc Inst Mech Eng Part J J Eng Tribol 2001;215:339–52.

[22] Degroote J, Bathe K-J, Vierendeels J. Performance of a new partitioned procedure versus a monolithic procedure in fluid–structure interaction. Comput Struct 2009;87:793–801.

[23] Degroote J. Partitioned simulation of fluid-structure interaction. Arch Comput Methods Eng 2013;20:185–238.

[24] Cardiff P, Karač A, De Jaeger P, Jasak H, Nagy J, Ivanković A, et al. An open-source finite volume toolbox for solid mechanics and fluid-solid interaction simulations. ArXiv Prepr ArXiv180810736 2018.

[25] Tuković Ž, Karač A, Cardiff P, Jasak H, Ivanković A. OpenFOAM finite volume solver for fluid-solid interaction. Trans FAMENA 2018;42:1–31.

[26] Cardiff P, Demirdžić I. Thirty years of the finite volume method for solid mechanics. Arch Comput Methods Eng 2021:1–60.

[27] Bair S. Reference liquids for quantitative elastohydrodynamics: selection and rheological characterization. Tribol Lett 2006;22:197–206.

[28] Bair S, Winer WO. The high pressure high shear stress rheology of liquid lubricants 1992.

[29] Björling M, Habchi W, Bair S, Larsson R, Marklund P. Friction reduction in elastohydrodynamic contacts by thin-layer thermal insulation. Tribol Lett 2014;53:477–86.

[30] Srirattayawong S. CFD study of surface roughness effects on the thermo-elastohydrodynamic lubrication line contact problem 2014.

[31] Tošić M. Model of Thermal EHL Based on Navier-Stokes Equations: Effects of Asperities and Extreme Loads 2019.

[32] Tošić M, Larsson R, Jovanović J, Lohner T, Björling M, Stahl K. A Computational Fluid Dynamics Study on Shearing Mechanisms in Thermal Elastohydrodynamic Line Contacts. Lubricants 2019;7:69.